Supporting Information

Complete Complex Amplitude Modulation with Electronically Tunable Graphene Plasmonic Metamolecules

Sangjun Han,[†,#] Seyoon Kim,[‡,#,*] Shinho Kim,[†] Tony Low,[§] Victor Watson Brar,[‡] and Min Seok Jang[†,*]

[*]Se.K: skim886@wisc.edu

[*]M.S.J: jang.minseok@kaist.ac.kr

[#]Equally contributed authors

[†]School of Electrical Engineering, Korea Advanced Institute of Science and Technology, Daejeon 34141, Korea

[‡]Department of Physics, University of Wisconsin-Madison, Madison, WI 53606, USA

[§]Department of Electrical & Computer Engineering, University of Minnesota, Minneapolis, MN 55455, USA

Contents

Supporting Figures

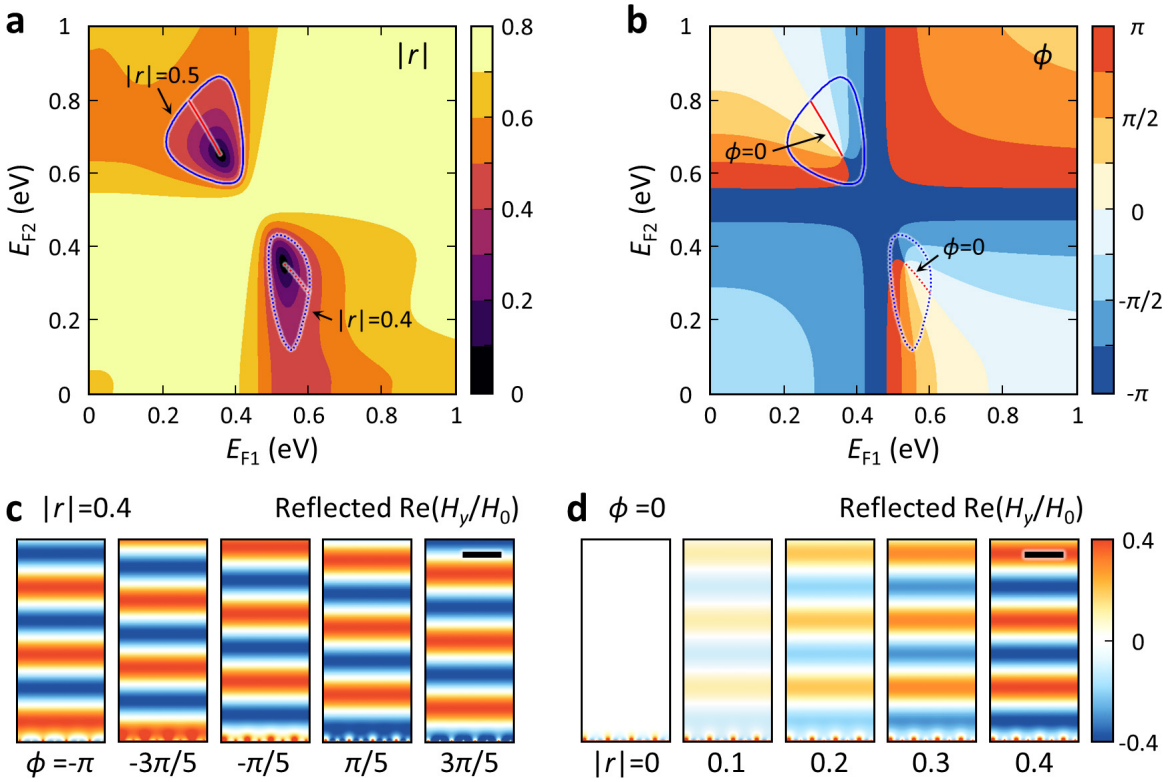

Figure S1. (a) Amplitude ($|r|$) and (b) phase (ϕ) of the reflection coefficient ($|r|e^{i\phi}$) as functions of the graphene Fermi levels (E_{F1} and E_{F2}) of the metaatoms. Reflected transverse magnetic field components (H_y) displaying (c) phase modulation with a constant amplitude ($|r|$=0.4) along the dotted blue line and (d) amplitude modulation with a constant phase (ϕ=0) along the dotted red line. In (c) and (d), the scale bars are 4 μm, and the graphene Fermi levels (E_{F1} and E_{F2}) used in the calculations are presented in Table S2.

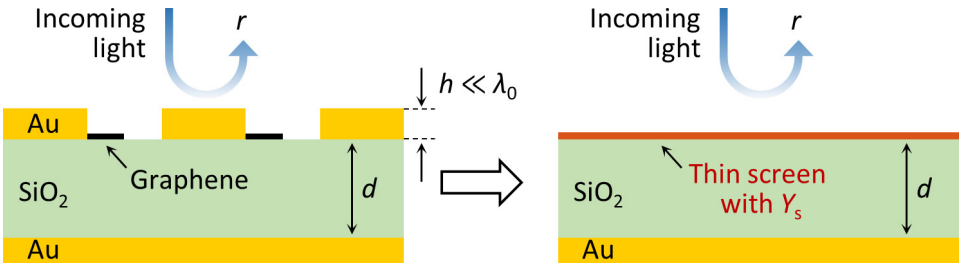

Figure S2. Graphene plasmonic metaatoms can be modeled by surface admittance (Y_s) if the thickness (h) is much thinner than a free space wavelength (λ_0).

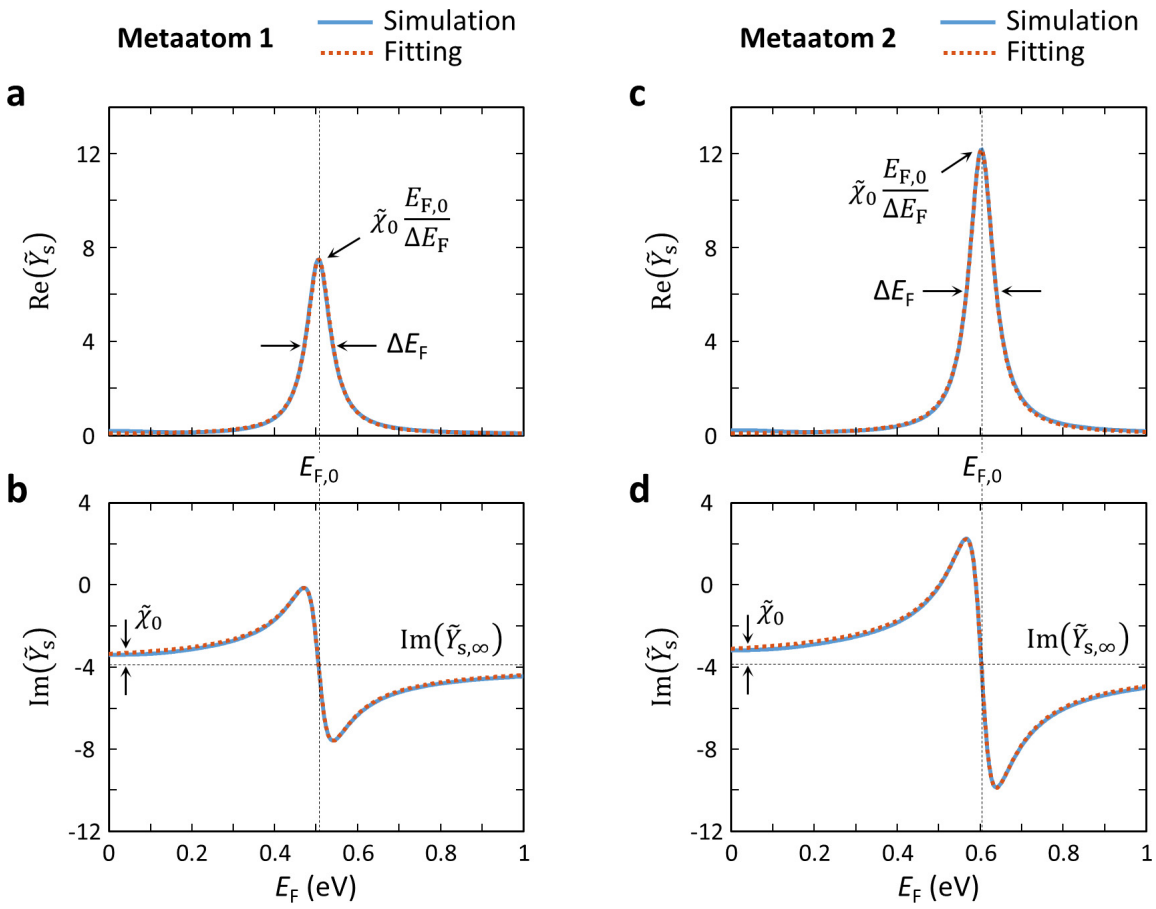

Figure S3. (a) The real part and (b) the imaginary part of the surface admittance of the metaatom 1. The fitting parameters for the modified susceptibility model in eq S3 are $\tilde{Y}_{s,\infty}$=0.047−3.88*i*, $\tilde{\chi}_0$=1.03, $E_{F,0}$=0.506 eV, and ΔE_F=0.070 eV. (c) The real part and (d) the imaginary part of the surface admittance of the metaatom 2. The fitting parameters for the modified susceptibility model in eq S3 are $\tilde{Y}_{s,\infty}$=0.046−3.84*i*, $\tilde{\chi}_0$=1.45, $E_{F,0}$=0.603 eV, and ΔE_F=0.072 eV.

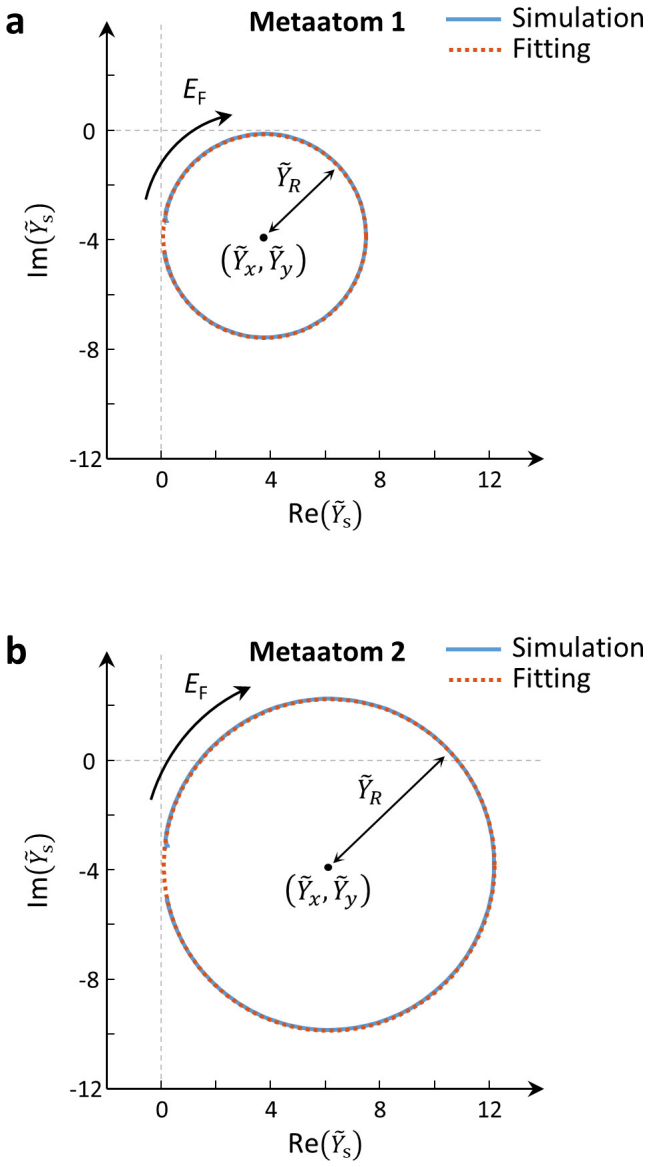

Figure S4. (a) The surface admittance of the metaatom 1 and (b) the surface admittance of the metaatom 2 calculated by full-wave simulations (solid blue lines) and by fitting with circles (dotted red lines). In the full-wave simulations, the graphene Fermi levels are tuned from zero to 1 eV. The circles were evaluated by eqs S4 and S5 with the parameters ($\tilde{Y}_{s,\infty}$, $\tilde{\chi}_0$, $E_{F,0}$, and ΔE_F) given in Figure S3. The circle parameters are $(\tilde{Y}_x, \tilde{Y}_y, \tilde{Y}_R)$=(3.77, −3.88, 3.72) for the metaatom 1 and $(\tilde{Y}_x, \tilde{Y}_y, \tilde{Y}_R)$=(6.10, −3.84, 6.06) for the metaatom 2.

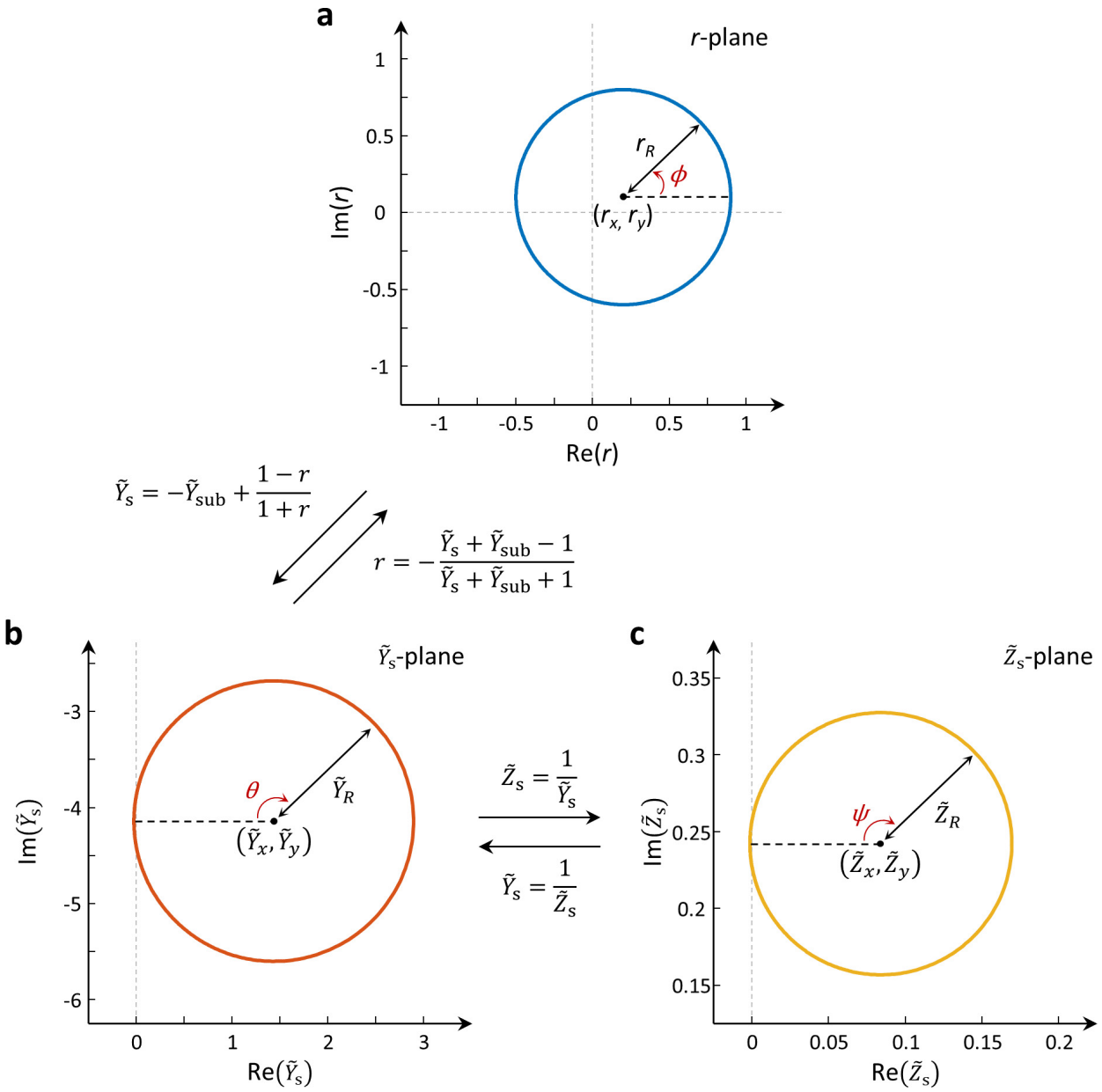

Figure S5. Schematic of conformal mapping among (a) reflection coefficient $r = \left(r_x + r_R \cos\phi\,, r_y + r_R \sin\phi\right)$ evaluated with (r_x, r_y, r_R)=(0.2, 0.1, 0.7), (b) corresponding surface admittance $\tilde{Y}_s = \left(\tilde{Y}_x - \tilde{Y}_R \cos\theta\,, \tilde{Y}_y + \tilde{Y}_R \sin\theta\right)$, and (c) corresponding surface impedance $\tilde{Z}_s = \left(\tilde{Z}_x - \tilde{Z}_R \cos\psi\,, \tilde{Z}_y + \tilde{Z}_R \sin\psi\right)$. The subscripts *x*, *y*, and *R* indicate the *x* position of center, the *y* position of center, and the radius of circle on a complex plane, respectively.

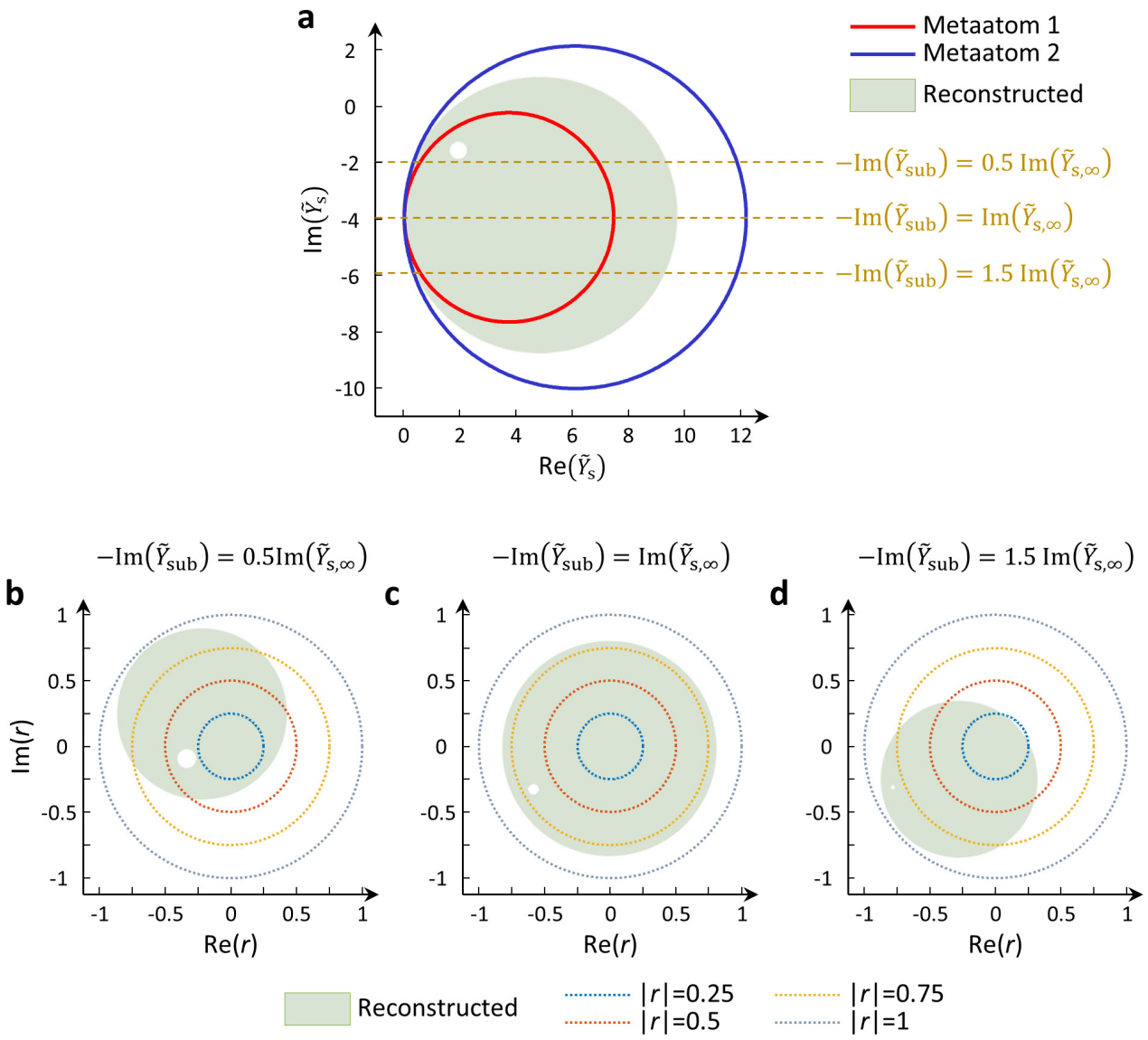

Figure S6. (a) Reconstructed surface admittance area (the shaded area) from the two metaatoms (the solid colored lines). (b-d) Reconstructed complex amplitude areas depending on the substrate admittance.

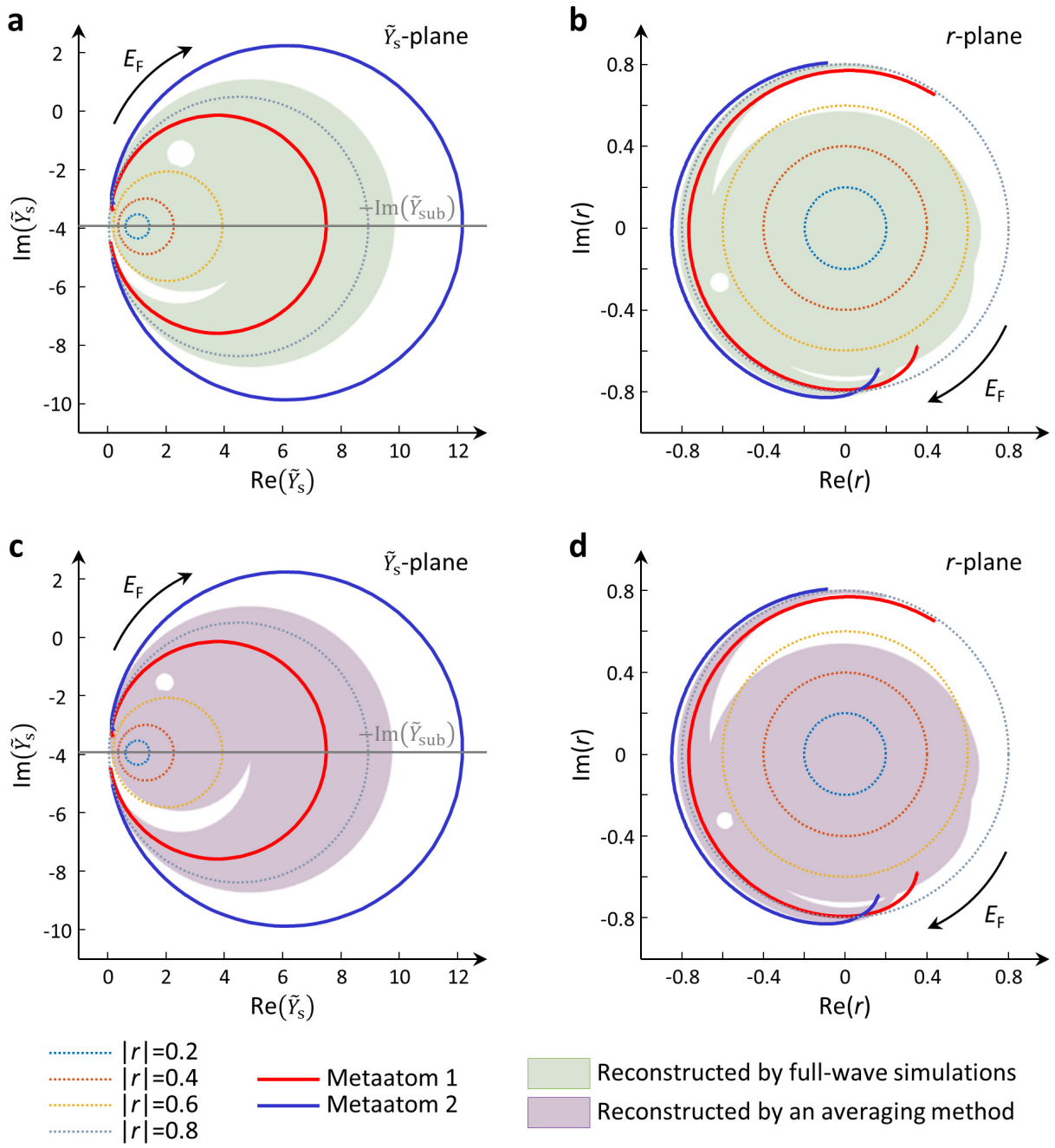

Figure S7. (a) Reconstructed surface admittance area and (b) reconstructed complex amplitude area by full-wave simulations. (c) Reconstructed surface admittance area and (d) reconstructed complex amplitude area by the weighted harmonic mean of the two metaatoms (the solid colored lines).

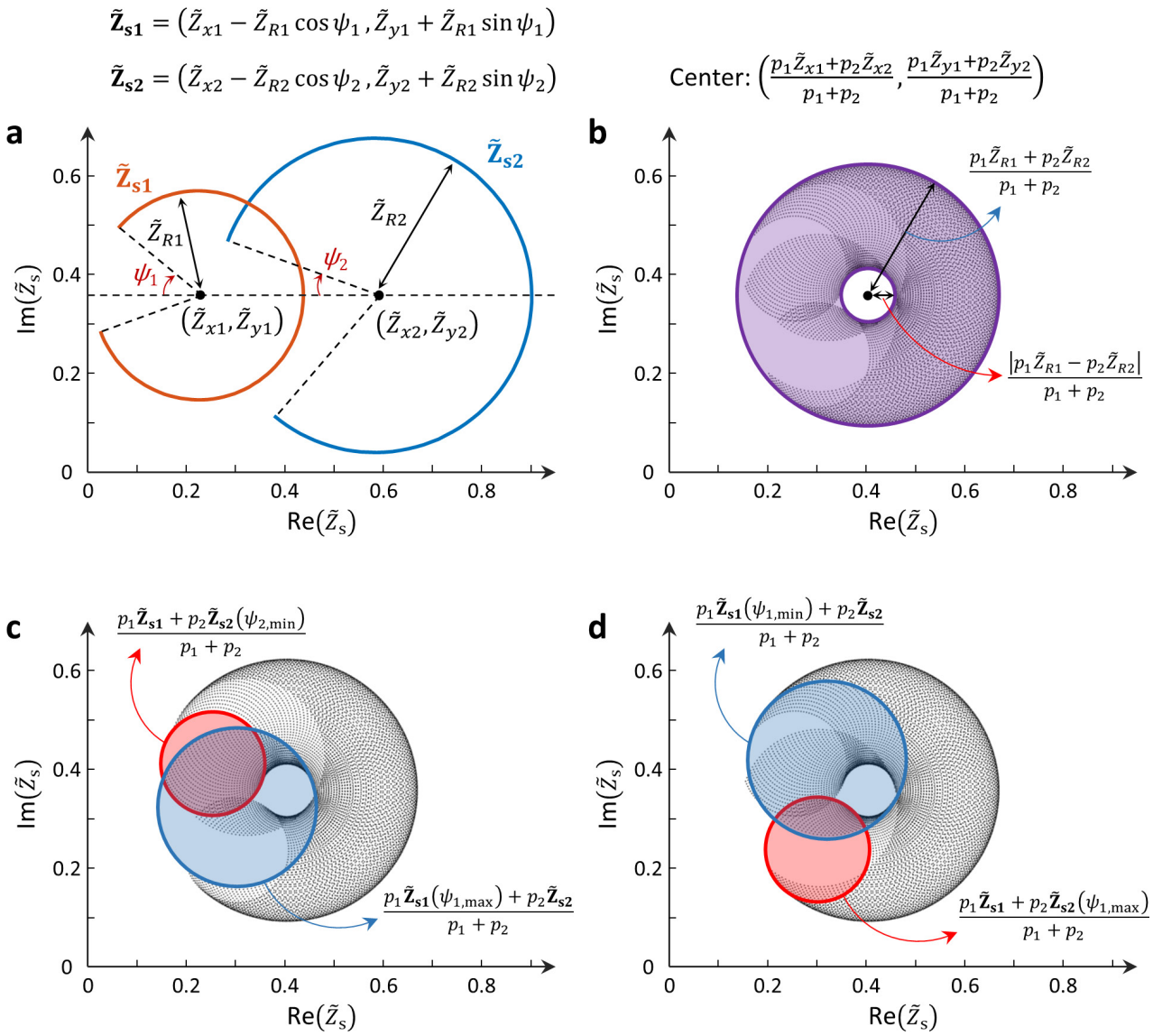

Figure S8. (a) Two arbitrary surface impedances denoted by $\tilde{\mathbf{Z}}_{\mathbf{s1}}$ and $\tilde{\mathbf{Z}}_{\mathbf{s2}}$. The polar angles are assumed to range from $\psi_{i,\min}$ to $\psi_{i,\max}$ (i=1,2). (b) The purple shaded area corresponds to the ideally reconstructed area when the two surface impedances form closed circles instead of arcs, and the dotted area is reconstructed by the actual metaatoms presented in (a). The center void arises from the weighted arithmetic mean of the two surface impedances, and this can be eliminated by balancing the pitches and the radii of the surface impedances. (c-d) Circles that determine the boundary of the metamolecule surface impedance coverage considering the limited tuning range.

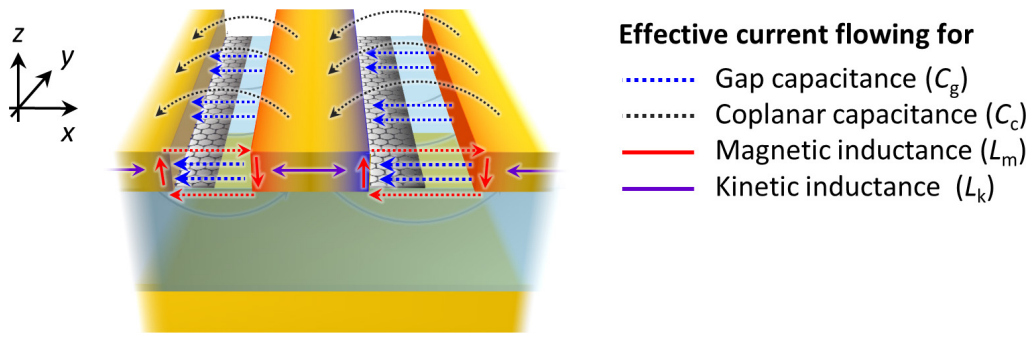

Figure S9. Schematic of effective current flowing for circuit elements.

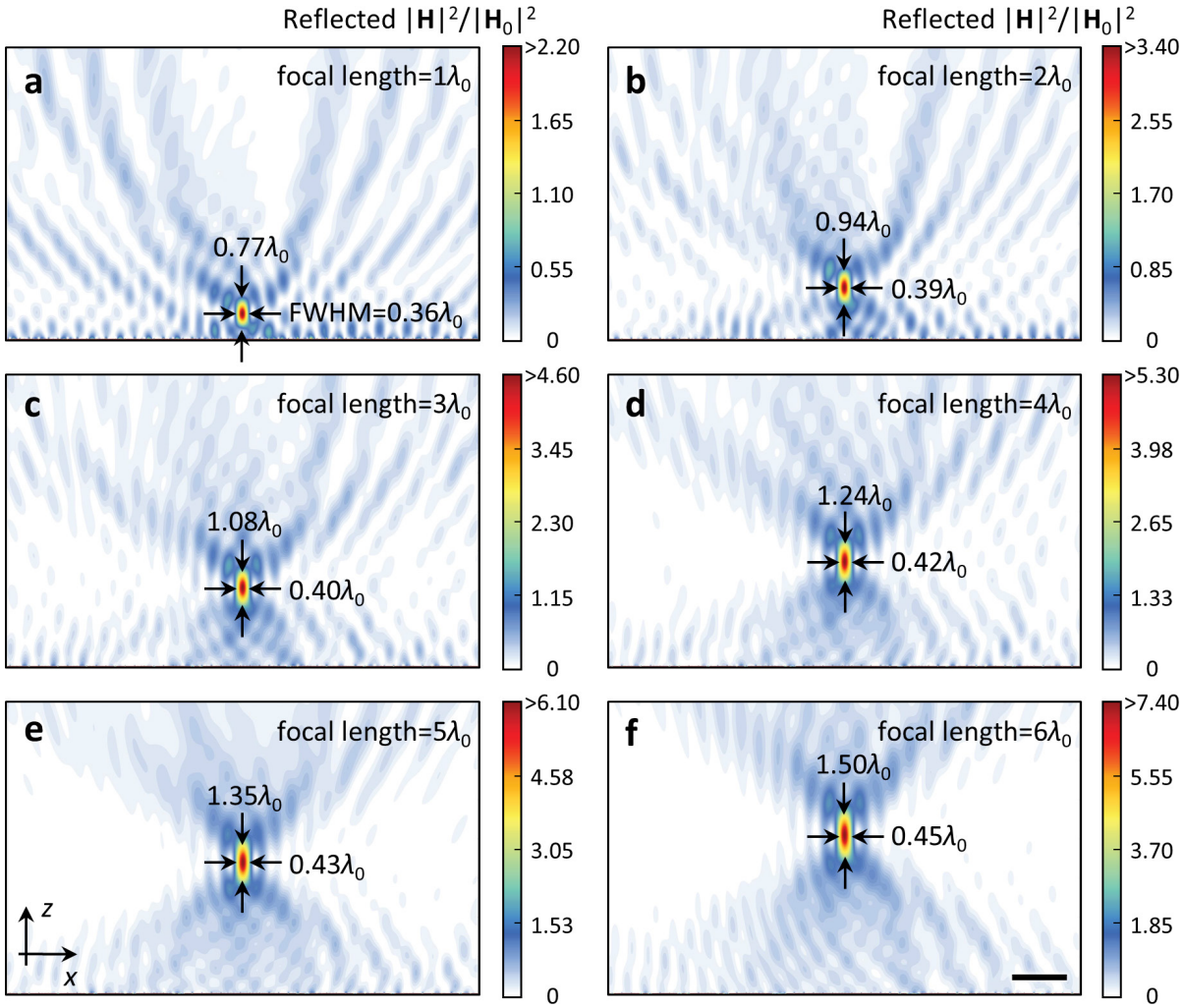

Figure S10. Reflected magnetic intensity distribution of beam single focusing with (a) $1\lambda_0$, (b) $2\lambda_0$, (c) $3\lambda_0$, (d) $4\lambda_0$, (e) $5\lambda_0$, and (f) $6\lambda_0$ focal lengths. In (a)-(f), full width at half maximums (FWHM) along *x* and *z* direction are denoted for each case and scale bar is 15 μm.

Supporting Tables

Table S1. Graphene Fermi levels used in Figure 1d,e.

Constant amplitude with $\|r\|$=0.5		
ϕ (rad)	E_{F1} (eV)	E_{F2} (eV)
$-\pi$	0.369	0.571
$-3\pi/5$	0.395	0.826
$-\pi/5$	0.316	0.842
$\pi/5$	0.236	0.750
$3\pi/5$	0.222	0.650

Constant phase with ϕ=0		
$\|r\|$	E_{F1} (eV)	E_{F2} (eV)
0	0.362	0.647
0.1	0.352	0.666
0.2	0.339	0.689
0.3	0.324	0.715
0.4	0.303	0.750

Table S2. Graphene Fermi levels used in Figure S1c,d.

Constant amplitude with $\|r\|$=0.4		
ϕ (rad)	E_{F1} (eV)	E_{F2} (eV)
$-\pi$	0.494	0.327
$-3\pi/5$	0.551	0.419
$-\pi/5$	0.603	0.329
$\pi/5$	0.590	0.210
$3\pi/5$	0.545	0.123

Constant phase with ϕ=0		
$\|r\|$	E_{F1} (eV)	E_{F2} (eV)
0	0.534	0.352
0.1	0.546	0.340
0.2	0.561	0.323
0.3	0.579	0.301
0.4	0.602	0.272

Table S3. Structure parameters used in Figure 5. For all structures, h and d are 80 nm, and 250 nm, respectively.

μ (cm^2 V^{-1} s^{-1})	p_1 (nm)	g_1 (nm)	w_1 (nm)	p_2 (nm)	g_2 (nm)	w_2 (nm)
500	1261	90	50	1006	60	40
1000	1470	120	55	1295	90	45
2000	1453	110	45	1200	80	45
4000	1379	100	45	1470	120	55

Supporting Notes

Note S1. Surface admittance

Assuming that the thickness of a graphene plasmonic metaatom is much thinner than free space wavelength, the structure can be modeled by a thin screen located at z=0 with effective surface admittance Y_s, as shown in Figure S2 (ref 1). Given a reflection coefficient in this schematic, a normalized surface admittance ($\tilde{Y}_s$) is evaluated by eq S1. The normalized substrate admittance ($\tilde{Y}_{sub}$) is determined by the structural geometries and the dielectric constants of the substrate, as given in eq S2.

$$\tilde{Y}_s = \frac{Y_s}{Y_0} = -\tilde{Y}_{sub} + \frac{1-r}{1+r} \tag{S1}$$

$$\tilde{Y}_{sub} = \frac{Y_{sub}}{Y_0} = \frac{n_{Au} - in_{SiO_2}\tan(n_{SiO_2}k_0 d)}{1 - i\left(n_{Au}/n_{SiO_2}\right)\tan(n_{SiO_2}k_0 d)} \tag{S2}$$

Here, Y_0, n_{Au}, n_{SiO2}, k_0, and d are the free space admittance, the refractive indices of the Au back reflector, the SiO_2 insulating layer, the wavenumber of free space light, and the thickness of the insulating layer, respectively. Au is nearly a perfect conductor in the mid-infrared, and there is no optical phonon in SiO_2 at a free space wavelength of 7 μm. Therefore, there is negligible absorption in the substrate, and the substrate admittance can be considered as a purely imaginary value.

Since the graphene plasmonic resonance in metaatoms is a type of dipolar resonance, the metaatoms exhibit Lorentzian lineshape as a function of graphene Fermi levels. Based on this property, we adopted a susceptibility model to describe the surface admittance term in our previous work.[1] In the viewpoint of a susceptibility model, the difference between graphene plasmonic metaatoms and dispersive materials is that the surface admittance is a function of graphene Fermi levels instead of frequency in a dielectric function. Here, we point out that the surface admittances of graphene plasmonic metaatoms appear as circles on a surface admittance plane owing to their Lorentzian resonance, and more details will be discussed later. The surface admittance based on a modified susceptibility model is described as

$$\tilde{Y}_s(E_F) = \tilde{Y}_{s,\infty} + i\tilde{\chi}(E_F) = \tilde{Y}_{s,\infty} + i\tilde{\chi}_0 \frac{E_{F,0}/2}{\left(E_{F,0} - E_F\right) + i\Delta E_F/2} \tag{S3}$$

where $\tilde{Y}_{s,\infty}$ is the normalized surface admittance at an infinite graphene Fermi level limit similar to permittivity at high frequency in the Debye model,[2] $\tilde{\chi}_0$ represents the plasmonic oscillator strength in graphene, $E_{F,0}$ is the graphene Fermi level at a resonance, and ΔE_F is the linewidth in graphene Fermi level. In the resonant medium model, the real and imaginary part of the susceptibility are related to the refractive index of a medium and the absorption,[3] respectively. Therefore, the surface admittance is multiplied by i to match the real and imaginary part of the resonant medium model with the surface conductance and surface susceptance of the graphene plasmonic metaatom, respectively. We adopted $\tilde{\chi}(E_F)$ as a reduced susceptibility near resonance instead of a full

susceptibility expression to account for the Lorentzian lineshape in the surface conductance originated from dipolar plasmonic resonance.[3,4] Here, the $i\tilde{\chi}(E_{\mathrm{F}})$ term is responsible for producing a circle on a surface admittance plane. The fitting results of the metaatoms given in the manuscript are presented in Figure S3. In complex $\tilde{Y}_{\mathrm{s}}$-plane, their trajectories are displayed as circles, as shown in Figure S4.

At a very high graphene Fermi level, there is negligible plasmonic absorption in graphene. In addition, absorption in noble metal structure is not significant because novel metals are almost perfect conductors in the mid-infrared as well as far away from the strong intrinsic noble metal plasmonic resonance, which appears in the visible range. Therefore, the $\tilde{Y}_{\mathrm{s},\infty}$ can be also approximated by a purely imaginary value likewise the substrate admittance ($\tilde{Y}_{\mathrm{sub}}$), and the $\tilde{Y}_{\mathrm{s},\infty}$ acts as an imaginary offset of the circular surface admittance. For this reason, we call the $\tilde{Y}_{\mathrm{s},\infty}$ as a "net surface admittance", and the $\tilde{Y}_{\mathrm{s},\infty}$ represents the surface susceptance when the surface conductance is maximized. The real part and the imaginary part of eq S3 are derived as follows.

$$\begin{aligned}\mathrm{Re}\left(\tilde{Y}_{\mathrm{S}}(E_{\mathrm{F}})\right) &= \mathrm{Re}\left(\tilde{Y}_{\mathrm{s},\infty}\right) + \frac{\tilde{\chi}_0 E_{\mathrm{F},0}}{2\Delta E_{\mathrm{F}}} - \frac{\tilde{\chi}_0 E_{\mathrm{F},0}}{2\Delta E_{\mathrm{F}}}\frac{\left(E_{\mathrm{F},0}-E_{\mathrm{F}}\right)^2-(\Delta E_{\mathrm{F}}/2)^2}{\left(E_{\mathrm{F},0}-E_{\mathrm{F}}\right)^2+(\Delta E_{\mathrm{F}}/2)^2} \\ &= \left[\mathrm{Re}\left(\tilde{Y}_{\mathrm{s},\infty}\right) + \frac{\tilde{\chi}_0 E_{\mathrm{F},0}}{2\Delta E_{\mathrm{F}}}\right] - \frac{\tilde{\chi}_0 E_{\mathrm{F},0}}{2\Delta E_{\mathrm{F}}}\cos\left(\theta(E_{\mathrm{F}})\right),\end{aligned} \tag{S4}$$

$$\begin{aligned}\mathrm{Im}\left(\tilde{Y}_{\mathrm{S}}(E_{\mathrm{F}})\right) &= \mathrm{Im}\left(\tilde{Y}_{\mathrm{s},\infty}\right) + \frac{\tilde{\chi}_0 E_{\mathrm{F},0}}{2\Delta E_{\mathrm{F}}}\frac{\Delta E_{\mathrm{F}}\left(E_{\mathrm{F},0}-E_{\mathrm{F}}\right)}{\left(E_{\mathrm{F},0}-E_{\mathrm{F}}\right)^2+(\Delta E_{\mathrm{F}}/2)^2} \\ &= \mathrm{Im}\left(\tilde{Y}_{\mathrm{s},\infty}\right) + \frac{\tilde{\chi}_0 E_{\mathrm{F},0}}{2\Delta E_{\mathrm{F}}}\sin\left(\theta(E_{\mathrm{F}})\right).\end{aligned} \tag{S5}$$

Here, we define a polar angle, $\theta(E_{\mathrm{F}})$, which is measured clockwise from the real axis (see Figure S5b). Thus, the surface admittance is mapped into a circle with a radius of $\tilde{\chi}_0 E_{\mathrm{F},0}/(2\Delta E_{\mathrm{F}})$ and a center position of $\left(\mathrm{Re}\left(\tilde{Y}_{\mathrm{s},\infty}\right)+\tilde{\chi}_0 E_{\mathrm{F},0}/(2\Delta E_{\mathrm{F}}),\mathrm{Im}\left(\tilde{Y}_{\mathrm{s},\infty}\right)\right)$ assuming the graphene Fermi level can be freely tuned from zero to infinity. As shown in Figure S4, the surface admittances calculated by full-wave simulations are accurately fitted with the circular trajectories owing to their Lorentzian lineshape. The circles were evaluated by eqs S4-S5 with the parameters of $\tilde{Y}_{\mathrm{s},\infty}$, $\tilde{\chi}_0$, $E_{\mathrm{F},0}$, and ΔE_{F} given in Figure S3. In particular, eq S5 confirms that the net surface admittance $\tilde{Y}_{\mathrm{s},\infty}$ corresponds to the imaginary offset of a circular trajectory considering the negligible $\mathrm{Re}\left(\tilde{Y}_{\mathrm{s},\infty}\right)$.

Note S2. Relation among reflection coefficient, surface admittance, and surface impedance

When a pair of metaatoms are alternately arranged, the effective surface admittance ($\tilde{Y}_\mathrm{s}$), and surface impedance ($\tilde{Z}_\mathrm{s}$) of the metamolecule are as follows.

$$\tilde{Y}_\mathrm{s} = \left(\frac{p_1/\tilde{Y}_{\mathrm{s}1} + p_2/\tilde{Y}_{\mathrm{s}2}}{p_1 + p_2}\right)^{-1} \tag{S6}$$

$$\tilde{Z}_\mathrm{s} = \frac{p_1\tilde{Z}_{\mathrm{s}1} + p_2\tilde{Z}_{\mathrm{s}2}}{p_1 + p_2} \tag{S7}$$

where p is the period of the metaatoms, and the numbers in the subscription indicate metaatoms 1 and 2. The surface impedance approach allows us to intuitively estimate the boundary of the reconstructed area because the effective surface impedance is evaluated by weighted arithmetic mean of the metaatoms instead of weighted harmonic mean in calculating the effective surface admittance. In addition, the surface impedance enables analytic evaluation of the reconstructed area when a pair of metaatoms constitute a meatsurface, and more details will be discussed in Note S3.

In this section, we will show that the trajectories of surface admittances and surface impedances can be conformally mapped into circles on their complex planes when the corresponding complex reflection coefficient has a form of $|r|e^{i\phi}$, where $|r|$ is the amplitude and ϕ is the phase of the reflection. Figure S5 shows the schematic of conformal mapping among complex amplitude (r), surface admittance ($\tilde{Y}_\mathrm{s}$), and surface impedance ($\tilde{Z}_\mathrm{s}$). The complex amplitude, the surface admittance, and the surface impedance are expressed by $r = \left(r_x + r_R\cos\phi\,, r_y + r_R\sin\phi\right)$, $\tilde{Y}_\mathrm{s} = \left(\tilde{Y}_x - \tilde{Y}_R\cos\theta\,, \tilde{Y}_y + \tilde{Y}_R\sin\theta\right)$, and $\tilde{Z}_\mathrm{s} = \left(\tilde{Z}_x - \tilde{Z}_R\cos\psi\,, \tilde{Z}_y + \tilde{Z}_R\sin\psi\right)$, respectively. Here, the subscriptions x, y, and R indicate the x position of center, the y position of center, and the radius of circle on a complex plane, respectively. The polar angles ϕ, θ, and ψ and their directions are illustrated in Figure S5.

The conversion from the complex amplitude to the surface admittance is derived as follows.

$$\tilde{Y}_x = \frac{2(r_x+1)}{(r_x+1)^2 + r_y^2 - r_R^2} - \mathrm{Re}\left(\tilde{Y}_\mathrm{sub}\right) - 1 \tag{S8-a}$$

$$\tilde{Y}_y = -\frac{2r_y}{(r_x+1)^2 + r_y^2 - r_R^2} - \mathrm{Im}\left(\tilde{Y}_\mathrm{sub}\right) \tag{S8-b}$$

$$\tilde{Y}_R = \left|\frac{2r_R}{(r_x+1)^2 + r_y^2 - r_R^2}\right| \tag{S8-c}$$

$$\theta = \tan^{-1}\left\{\frac{2r_y\left[(r_x+1)^2+r_y^2+r_R^2+(r_x+1)r_R\cos\phi\right]+r_R\left[(r_x+1)^2+3r_y^2+r_R^2\right]\sin\phi}{r_R\left[-(r_x+1)^2+r_y^2+r_R^2\right]\cos\phi - 2(r_x+1)r_y r_R\sin\phi}\right\} \tag{S8-d}$$

The conversion from the surface admittance to the complex amplitude is derived as follows.

$$r_x = \frac{2Y_0^2\tilde{Y}_\alpha}{\tilde{Y}_\alpha^2 + \tilde{Y}_\beta^2 - \tilde{Y}_R^2} - 1 \tag{S9-a}$$

$$r_y = -\frac{2Y_0^2\tilde{Y}_\beta}{\tilde{Y}_\alpha^2 + \tilde{Y}_\beta^2 - \tilde{Y}_R^2} \tag{S9-b}$$

$$r_R = \left|\frac{2Y_0^2\tilde{Y}_R}{\tilde{Y}_\alpha^2 + \tilde{Y}_\beta^2 - \tilde{Y}_R^2}\right| \tag{S9-c}$$

$$\phi = \tan^{-1}\left[\frac{2\tilde{Y}_R\tilde{Y}_\beta - 2\tilde{Y}_\alpha\tilde{Y}_\beta\cos\theta + \left(\tilde{Y}_R^2 - \tilde{Y}_\alpha^2 + \tilde{Y}_\beta^2\right)\sin\theta}{\left(\tilde{Y}_\alpha^2 - \tilde{Y}_\beta^2 + \tilde{Y}_R^2\right)\cos\theta - 2\tilde{Y}_\alpha\left(\tilde{Y}_R + \tilde{Y}_\beta\sin\theta\right)}\right] \tag{S9-d}$$

where $\tilde{Y}_\alpha = 1 + \tilde{Y}_x + \mathrm{Re}\left(\tilde{Y}_{\mathrm{sub}}\right)$ and $\tilde{Y}_\beta = \tilde{Y}_y + \mathrm{Im}\left(\tilde{Y}_{\mathrm{sub}}\right)$.

The conversion from the surface admittance to the surface impedance is derived as follows.

$$\tilde{Z}_x = \frac{\tilde{Y}_x}{\tilde{Y}_x^2 + \tilde{Y}_y^2 - \tilde{Y}_R^2} \tag{S10-a}$$

$$\tilde{Z}_y = -\frac{\tilde{Y}_y}{\tilde{Y}_x^2 + \tilde{Y}_y^2 - \tilde{Y}_R^2} \tag{S10-b}$$

$$\tilde{Z}_R = \left|\frac{\tilde{Y}_r}{\tilde{Y}_x^2 + \tilde{Y}_y^2 - \tilde{Y}_R^2}\right| \tag{S10-c}$$

$$\psi = \tan^{-1}\left[\frac{-2\tilde{Y}_R\tilde{Y}_y + 2\tilde{Y}_x\tilde{Y}_y\cos\theta - \left(\tilde{Y}_R^2 - \tilde{Y}_x^2 + \tilde{Y}_y^2\right)\sin\theta}{\left(\tilde{Y}_x^2 - \tilde{Y}_y^2 + \tilde{Y}_R^2\right)\cos\theta - 2\tilde{Y}_x\left(\tilde{Y}_R + \tilde{Y}_y\sin\theta\right)}\right] \tag{S10-d}$$

The conversion from the surface impedance to the surface admittance is derived as follows.

$$\tilde{Y}_x = \frac{\tilde{Z}_x}{\tilde{Z}_x^2 + \tilde{Z}_y^2 - \tilde{Z}_R^2} \tag{S11-a}$$

$$\tilde{Y}_y = \frac{\tilde{Z}_y}{\tilde{Z}_x^2 + \tilde{Z}_y^2 - \tilde{Z}_R^2} \tag{S11-b}$$

$$\tilde{Y}_R = \left|\frac{\tilde{Z}_R}{\tilde{Z}_x^2 + \tilde{Z}_y^2 - \tilde{Z}_R^2}\right| \tag{S11-c}$$

$$\theta = \tan^{-1}\left[\frac{-2\tilde{Z}_R\tilde{Z}_y + 2\tilde{Z}_x\tilde{Z}_y\cos\psi - \left(\tilde{Z}_R^2 - \tilde{Z}_x^2 + \tilde{Z}_y^2\right)\sin\psi}{\left(\tilde{Z}_x^2 - \tilde{Z}_y^2 + \tilde{Z}_R^2\right)\cos\psi - \tilde{Z}_x\left(\tilde{Z}_R + \tilde{Z}_y\sin\psi\right)}\right] \tag{S11-d}$$

Note S3. Analysis of reconstructed surface impedance area

In an ideal case, the complex amplitude has to form a circle with (r_x,r_y)=(0,0), and this condition leads to $\tilde{Y}_y = -\mathrm{Im}(\tilde{Y}_{\mathrm{sub}})$ by eq S8-b. This requirement implies that the tunability of a metamolecule in *r*-plane is maximized when the imaginary part of the net surface admittance, $\mathrm{Im}(\tilde{Y}_{\mathrm{s},\infty})$, is aligned with the negative imaginary value of the substrate admittance, $-\mathrm{Im}(\tilde{Y}_{\mathrm{sub}})$. Figure S6 shows the reconstructed complex amplitude areas depending on the substrate admittance. In Figure S6a, the solid red and blue lines correspond to the surface admittance of the metaatoms, and the green shaded area is the surface admittance area reconstructed by independently tuning the metaatoms. As shown in Figure S6, the reconstructed area in r-plane is maximized when $-\mathrm{Im}(\tilde{Y}_{\mathrm{sub}}) = \mathrm{Im}(\tilde{Y}_{\mathrm{s},\infty})$, and the reconstructed area is shrunken and shifted when the substrate admittance deviates from the net surface admittance.

In Figure 2 of the manuscript and Figure S6,S7, there are circular voids inside the reconstructed areas even in the ideal case. The weighted harmonic mean of two metaatoms inevitably creates these voids in the reconstructed areas when the pitches of the metaatoms and the radii of the surface admittance trajectories are not balanced. In addition, the limited tunable graphene Fermi levels prevent the surface admittances from forming closed circles, and result in additional unfilled areas in the reconstructed regions. These voids and the unfilled areas can be analytically estimated by investigating their surface impedances.

Figure S8a shows two arbitrary surface impedances exhibiting incomplete circles due to the limited tuning range. The surface impedances of the two metaatoms are denoted by $\tilde{\mathbf{Z}}_{\mathbf{s1}}$ and $\tilde{\mathbf{Z}}_{\mathbf{s2}}$. Each trajectory is given by an arc with a radius of $\tilde{Z}_{Ri}$ and polar angle ranging from $\psi_{i,\min}$ to $\psi_{i,\max}$ (i=1,2). When we calculate the effective surface impedance area by the weighted arithmetic mean of the two metaatoms, the reconstructed area forms a partially filled circle, as presented by the black dots in Figure S8b-d.

When we examine the reconstructed area, we can identify six circles that bound the surface impedance of the metamolecule as presented in Figure S8b-d. The two circles presented as purple solid curves in Figure S8b determine the boundaries of the metamolecule's surface impedance coverage in ideal case (*i.e.*, each metaatom forms a closed circle in the surface impedance plane). Both circles are centered at the weighted arithmetic mean of the two metaatoms' impedance centers, and their radii are $(p_1\tilde{Z}_{R1} + p_2\tilde{Z}_{R2})/(p_1 + p_2)$ and $|p_1\tilde{Z}_{R1} - p_2\tilde{Z}_{R2}|/(p_1 + p_2)$. The inner void in the purple shaded area arises from an imbalance between two metaatoms and can be eliminated when $p_1\tilde{Z}_{R1} = p_2\tilde{Z}_{R2}$. The limited tuning range further constrains the metamolecules' impedance coverage, and its boundary is defined by the four circles identified in Figure S8c,d.

Note S4. Inter-coupling between the metaatoms

One could concern that there is significant inter-coupling between the adjacent metaatoms, and that such coupling will cause critical failures to our device. In fact, it is one of our major claims that a unit cell of metamolecule can be configured by neighboring two metaatoms because there is no strong inter-coupling between the adjacent resonators. There could be inter-coupling issues if the metal strips served as noble metal plasmonic resonators. However, our device design primarily relies on strong plasmonic resonances in the graphene nanoresonators, which support highly confined modes, hence extending a much smaller volume of their environment and the metal strips. The metal strips are exploited only to enhance the oscillator strength of the graphene nanoresonators *via* "non-resonant" focusing effects.[5] In other words, the metal strips do not take part in determining the resonance condition of the GPRs, such as resonant frequencies. This configuration results in optically isolated GPRs without inter-coupling issues.

If there is strong inter-coupling between the adjacent metaatoms, it should be observable in the electric field distributions. In addition, their magnitudes should be comparable to those of GPRs. However, there is no significant electric field inside the insulator or on top of the metal strips, as shown in Figure 1f,g of the manuscript. In particular, the electric field around the GPRs is overwhelmingly stronger than that of other regions. This clearly supports that there is no critical inter-coupling between the adjacent metaatoms.

Surface admittance model in our work more clearly describes the aforementioned characteristics. The main concept of the surface admittance model is that the metasurfaces can be represented by a thin screen with effective surface admittance. Then, electromagnetic behaviors of the whole structure can be modeled by simply stratified layers. This approach is valid only if there are no significant electromagnetic waves propagating into transverse directions, which should be responsible for the inter-coupling. The validity of this model is displayed in Figure S3-S4. The calculation results based on the surface admittance model show excellent agreement with full-wave simulation results.

To analyze the metasurface consisting of two metaatoms, we adopted the weighted harmonic mean of the two surface admittances. This approach is also only valid if there is no inter-coupling between the adjacent resonators because no interaction term between the two surface admittances is included in the weighted harmonic mean. In other words, only their collective electromagnetic responses are considered without interactions between them. The validity of this model is supported by Figure S7. In this calculations, we compared full-simulation results of a "full unit cell structure" and analytic calculations based on the weighted harmonic mean of the two surface admittances. As shown in Figure S7, they show excellent agreement. These comparisons presented in Figure S3, S4, and S7 clearly reveal that there is no critical inter-coupling issue between the adjacent resonators.

Note S5. Circuit analysis

The surface admittance of a metaatom is composed of the surface admittance of the metal strips and that of graphene plasmonic ribbons (GPRs). To estimate the surface admittances analytically, we model the structure as a collection of circuit elements in the electrostatic limit, recognizing the characteristic length of the structure is much shorter than the free space wavelength of the incident light. In this circuit analysis, we consider effective currents generated by normally incident transverse magnetic wave.

The normalized surface admittance of a metallic structure, $\tilde{Y}_{\mathrm{metal}}$, can be modeled as

$$\tilde{Y}_{\mathrm{metal}} = \frac{p}{Y_0}\left[-i\omega(L_{\mathrm{m}} + L_k) + \frac{1}{-i\omega\left(C_{\mathrm{c}} + C_{\mathrm{g}}\right)}\right]^{-1} \tag{S12}$$

where p is the pitch of the structure, ω is the operating frequency, and Y_0 is the free space surface admittance. The circuit of a metallic structure presented in Figure S9 consists of four circuit components: coplanar capacitance (C_{c}), gap capacitance (C_{g}), magnetic inductance (L_{m}), and kinetic inductance (L_{k}). The circuit components depending on the structural parameters are derived as follows.

$$C_{\mathrm{g}} = \varepsilon_0 \frac{h}{g} \tag{S13-a}$$

$$C_{\mathrm{c}} = \frac{(\varepsilon_{\mathrm{r,air}} + \varepsilon_{\mathrm{r,SiO_2}})\varepsilon_0}{\pi} \log\frac{p}{g} \tag{S13-b}$$

$$L_{\mathrm{m}} = \mu_0 h g \tag{S13-c}$$

$$L_{\mathrm{k}} = \frac{p - g}{\varepsilon_0 \delta\left(1 - \varepsilon_{\mathrm{r,Au}}\right)\omega^2} \tag{S13-d}$$

where p, g, and h are the pitch, the gap, and the thickness of the metallic structure, respectively, and δ is the skin depth into the metal. ε_0, μ_0, and ε_{r} are the vacuum permittivity, the vacuum permeability, and the relative permittivity of materials, respectively. Since the metasurface has translational symmetry in y-direction, the capacitive components (C_{c} and C_{g}) are defined as capacitance per y length and the inductive components (L_{m} and L_{k}) are defined as inductance times y length.

The coplanar capacitance (C_{c}) accounts for the capacitance between two infinitely thin metallic strips.[6] The gap capacitance (C_{g}) describes the gap between the metallic strips as a parallel plate capacitor with a width h and gap distance g. As the metallic structure becomes thinner and the gap becomes wider, the coplanar capacitance dominates over the gap capacitance.

The current flowing in the structure introduces non-negligible inductances, L_{m}, and L_{k}, as shown in Figure S9. The magnetic inductance L_{m} originates from the current circulating the gap between the two metal strips, denoted by red arrows in Figure S9. The kinetic inductance L_{k} arises from current flowing in x-direction in the metal strip, and it can be derived from a general expression of impedance[7] given in eq S14, and it leads to eq S13-d.

$$-i\omega L_{\mathrm{k1}} = \frac{1}{\sigma(\omega)}\frac{p-g}{\delta} = \frac{1}{-i\omega\varepsilon_0(\varepsilon_{\mathrm{Au}}-1)}\frac{p-g}{\delta}. \quad \text{(S14)}$$

Here, the skin depth of gold (δ) at free space wavelength 7 μm is about 27 nm, which is smaller than the thickness of the metal strip.

To model the effect of a GPR between the metal strips, we consider the GPR as a perfect two-dimensional system with an effective sheet conductivity. In addition, the presence of metal strips allows for the formation of virtual GPRs with image charges, effectively introducing an array of GPRs with a larger width and a shorter periodicity. This situation enables us to calculate the sheet conductivity of this composite nanostructure in a simpler manner. Each GPR can be modelled as a dipole whose dipole moment is defined as $p_e = \alpha E_{\mathrm{local}}$, where α is the polarizability of the GPR, and E_{local} is the local electric field.[8] The sheet polarization density, P, of the GPR array is expressed as:

$$P = \nu p_e = \nu\alpha E_{\mathrm{local}} = \chi E_0. \quad \text{(S15)}$$

Here, ν is the number of dipoles per unit area and E_0 is an electric field incident on the nanostructure. $\chi = \nu\alpha E_{\mathrm{local}}/E_0$ is the susceptibility of the GPR array. Assuming that the response of the GPR array follows the modified Drude-Lorentz model,[1,9] the normalized sheet conductivity, $\tilde{Y}_{\mathrm{A}}$, is expressed as:

$$\tilde{Y}_{\mathrm{A}} = -i\omega\frac{\chi}{Y_0} = -i\omega\nu\alpha\frac{E_{\mathrm{local}}}{Y_0 E_0} = \frac{E_{\mathrm{local}}}{E_0}\tilde{Y}_{\mathrm{GPR}} \quad \text{(S16)}$$

where $\tilde{Y}_{\mathrm{GPR}}$ is a normalized sheet conductivity of an array consisting of only GPRs without the metal strips. In this case, the E_0 equals the E_{local}. In the metaatoms, the E_{local} is enhanced due to the metal strips and that enhancement factor can be approximated as $E_{\mathrm{local}}/E_0 = p/g$, considering that the potential drop across the metallic strip is negligible compared to that across the gap.[5] Thus, the normalized sheet conductivity of the GPRs with the metal strip array is given by $(p/g)\tilde{Y}_{\mathrm{GPR}}$. Here, $\tilde{Y}_{\mathrm{GPR}}$ of a GPR array on a semi-infinite SiO_2 can also be calculated from the numerically obtained reflection coefficient r, as given in eq S17.

$$\tilde{Y}_{\mathrm{GPR}} = \frac{1-r}{1+r} - n_{\mathrm{SiO_2}} \quad \text{(S17)}$$

where n_{SiO2} is the refractive index of SiO_2. Considering the effects of the metal strips and the GPRs on the substrate simultaneously, we can obtain normalized total sheet admittance, $\tilde{Y}_{\mathrm{s,model}}$, which is given by

$$\tilde{Y}_{\mathrm{s,model}} = \tilde{Y}_{\mathrm{metal}} + \frac{p}{g}\tilde{Y}_{\mathrm{GPR}}. \quad \text{(S18)}$$

We note that $\tilde{Y}_{\mathrm{GPR}}$ is derived from the GPR array with period $2g$ and width $2w\times F$. Here, $2g$ and $2w$ are twice the metallic gap and the GPR width, respectively. This double widening effect is given in order to consider the image charges created by the metal strips. In addition, charges are accumulated at the junction of metal/graphene, which results in reducing the dipole field strength. Due to this effect, the GPR width effectively shrinks with a reduction factor F=0.942.

References

(1) Kim, S.; Jang, M. S.; Brar, V. W.; Mauser, K. W.; Kim, L.; Atwater, H. A. Electronically Tunable Perfect Absorption in Graphene. *Nano Lett.* **2018**, *18*, 971-979.

(2) Mantas, P. Q. Dielectric Response of Materials: Extension to the Debye Model. *J. Eur. Ceram. Soc.* **1999**, *19*, 2079-2086.

(3) Saleh, B. E. A.; Teich, M. C. *Fundamentals of Photonics*, 2nd ed.; Wiley: Hoboken, **2007**.

(4) Sönnichsen, C.; Franzl, T.; Wilk, T.; von Plessen, G.; Feldmann, J. Plasmon Resonances in Large Noble-Metal Clusters. *New J. Phys.* **2002**, *4*, 93.91-93.98.

(5) Novitsky, A.; Ivinskaya, A. M.; Zalkovskij, M.; Malureanu, R.; Jepsen, P. U.; Lavrinenko, A. V. Non-Resonant Terahertz Field Enhancement in Periodically Arranged Nanoslits. *J. Appl. Phys.* **2012**, *112*, 074318.

(6) Paul, C. R. *Analysis of Multiconductor Transmission Lines*, 2nd ed.; Wiley-IEEE Press: Hoboken, **2008**.

(7) Staffaroni, M.; Conway, J.; Vedantam, S.; Tang, J.; Yablonovitch, E. Circuit Analysis in Metal-Optics. *Photonics Nanostructures: Fundam. Appl.* **2012**, *10*, 166-176.

(8) Silveiro, I.; Ortega, J. M. P.; de Abajo, F. J. G. Plasmon Wave Function of Graphene Nanoribbons. *New J. Phys.* **2015**, *17*, 083013.

(9) Jadidi, M. M.; Konig-Otto, J. C.; Winnerl, S.; Sushkov, A. B.; Drew, H. D.; Murphy, T. E.; Mittendorff, M. Nonlinear Terahertz Absorption of Graphene Plasmons. *Nano Lett.* **2016**, *16*, 2734-2738.